VALIDATION OF AN ANALYTICAL MODEL DESCRIBING THE HEAT FLUX DISTRIBUTION IN LOAD-BEARING CFRP SINGLE-LAP JOINTS

Michael Lange [(1)], Volodymyr Baturkin [(2)], Christian Hühne [(1)], Olaf Mierheim [(1)]

[(1)] DLR, Lilienthalplatz 7, 38108, Braunschweig, Germany, Email: m.lange@dlr.de
[(2)] DLR, Robert-Hooke-Straße 7, 28359 Bremen, Germany, Email: volodymyr.baturkin@dlr.de

ABSTRACT

Usually, in phase 0/A the structural and thermal engineering are developed in parallel. But especially when developing a structure made from fibre reinforced plastics both subsystems influence each other because of the materials orthotropic nature. In order to allow a partially coupled analysis, the paper introduces into a semi-analytic formula which connects the structural and thermal analysis of load-bearing single-lap joints and is based on a shear-stress analogue description of the out-of-plane heat flux distribution in the adhesive layer. Further it is shown how from this a single-lap joint's thermal resistance could be derived. For validation, a formerly presented thermal vacuum test with single-lap joint specimens is repeated with improved setup and compared to an updated numerical model.

1. INTRODUCTION

It is common practice in space system engineering to apply in phase 0/A studies the concurrent design or concurrent engineering process. It demands a subsystem development which complies from the beginning on with its system-specific requirements but also interfaces equivalently well with the other subsystems [1]. This creates two major challenges when designing structures made of fibre reinforced plastics (FRP). Firstly in concurrent engineering studies design changes happen on a regular basis and secondly FRP composite structures usually have anisotropic material properties. Also, structural and (conductive) thermal loads often share the same paths in a structure. Consequently, a change in the materials properties, for instance by increasing a laminate's fibre volume content, does not only affect the structure's effective mechanical properties but also its effective thermal properties.

This close relation between structural and thermal design suggests a partially coupled analysis which is applied in early project phases. It should provide a systematic and comprehensive approach that allows the design of FRP structures with specific directional thermal conductivities or to run 'what if' type simulations for the assessment of variations in the laminate build-up on the global conductivities [2].

Therefore Lange proposed in [3] a combined 2D/3D FE simulation technique. It is based on primarily 2D elements for classical structural analysis and refined with 3D elements in regions with relevant out-of-plane (OOP) heat fluxes, id est joints and interfaces. The most crucial information lacking for such a modelling are the joints' effective thermal conductivities or thermal resistances. Having these determined they can be considered together with the known in-plane thermal conductivities (resistances) [4] in a combined structural-thermal model for concurrent engineering purposes and reliably implemented into the detailed thermal control systems design [5].

For the determination of the joints' thermal resistances Lange investigated exemplarily on three test coupons the steady-state temperature distributions in single-lap jointed (SLJ) carbon FRP (CFRP) laminates setup at room temperature in a thermal vacuum chamber. It was found that the analytically and numerically calculated temperature distribution in the specimens agrees for two of three cases well, whereas the third one and a corresponding validation experiment showed significant discrepancies. These are partially attributed to an insufficient experimental setup.

Hence, the central concern of the present paper's first part (section 2) is to present the results of the experiment as conducted in [3], but with improved setup. For that it is necessary to analyse the deficiencies of the former thermal vacuum test setup and to introduce a correspondingly improved one before the validation experiments are repeated. Then, for final validation, the present results are compared to the former experiments and numerical calculations.

The focus of the paper's second part (section 3) is the discrepancy found in one case (specimen #2, cf [3]) between the numerical and analytical calculation of the temperature drop over a SLJ and the connected thermal resistance. As proposed in [3], a semi-analytical model is investigated which is based on a shear stress-analogue description and allows the general calculation of the heat flux distribution within the SLJ. It will be explored how it meets the numerical simulations and how it further will eventually allow the determination of any SLJ's thermal resistance and the connected temperature drop through characteristic OOP heat flux peaks.

2. VALIDATION OF THE HEAT FLUX DISTRIBUTION AND THERMAL RESISTANCE ANALYSIS OF SLJs

In [3] Lange compared an analytical and numerical calculation of the x-directional temperature gradient along a glued CFRP SLJ and its thermal resistance respectively. Three specimen as listed in Tab. 1 were

Table 1: SLJ specimen design as designed and as manufactured.

Specimen Number	Specimen layout	Specimen geometry		
	Laminate-1 / Laminate-2	Param.	as designed	as manufact. (avg.)
			Reference Specimen	
#1	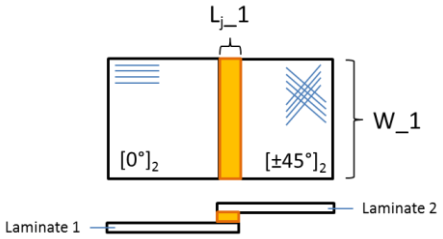	W_1 Lj_1 L_1 Lfl tlam1 tlam2 tglue	20 mm 10 mm 70 mm 15 mm 0.25 mm 0.5 mm 0.1 mm	20.05 mm - - - 0.271 mm 0.529 mm -
			Extension of overlapping length	
#2	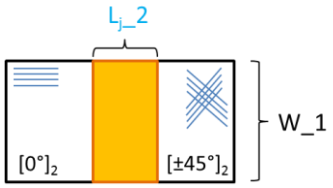	W_1 Lj_2 L_1 Lfl tlam1 tlam2 tglue	20 mm 20 mm 75 mm 15 mm 0.25 mm 0.5 mm 0.1 mm	20.03 mm - - - 0.260 mm 0.549 mm -
			Extension of overlapping width	
#3	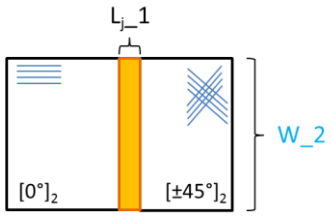	W_2 Lj_1 L_1 Lfl tlam1 tlam2 tglue	30 mm 10 mm 70 mm 15 mm 0.25 mm 0.5 mm 0.1 mm	30.02 mm - - - 0.273 mm 0.541 mm -

setup in a thermal vacuum chamber (residual gas pressure in chamber $p_{chamber}<5\cdot10^{-6}$ mbar), one end connected to a cold plate at 25°C and the other to a thermal resistance heater (cf Fig. 1). The temperatures were measured at six locations along the specimens. One Pt100 (1/3 DIN class B) temperature sensors (TS) was located at the cold plate flange and one at the heated flange. The other four sensors were located on the jointed CFRP laminates. It was shown in [3] that the analytical and numerical results agree for shorter jointed lengths (L_j=10 mm, specimen #1 and #3) quiet well, but deviate significantly for the longer one (L_j=20 mm, specimen #2). Further the experimental results showed a generally insufficient agreement amongst each other as well as in comparison to the numerical and analytical temperature analysis. Both observations are assigned to significant and inhomogeneous radiation effects in the thermal vacuum chamber, which were not considered in the numerical and analytical calculations.

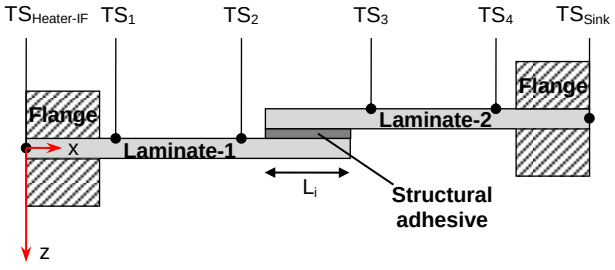

Figure 1: SLJ specimen with temperature sensors (TS) on the surface and controlled heater and clod plate (sink) temperature.

2.1. Deficiency analysis of the thermal vacuum test setup as in [3]

After identifying the aforementioned deviations in the thermal vacuum test analysis a following investigation [6] showed that the cylindrical thermal vacuum chamber vessel has a quite inhomogeneous temperature distribution with temperature differences of up to 4-5°C along the vessel's circumference. These are induced by the vacuum pump located close by at one side of the chamber and must be strictly avoided. Further:

- The three adjacently placed specimens can exchange heat via radiation (cf Fig. 2).
- Heater and sensor wires are connected by polyimide tape to the cold plate.
- The heater-sided flange and the resistance heater itself is not entirely covered by SLI (single-layer insulation foil).
- The resistance heater wire is not wrapped with SLI and not connected to the cold plate (temperature compensation). Also its cross section (AWG 22) is larger than required.
- No heat flux control within the specimen.

Therefore the following actions were taken in order to improve the thermal vacuum test setup and to minimise the radiative as well as conductive parasitic heat fluxes:

- Testing only one specimen at a time.
- Covering the specimen with an (inner) MLI, instead of eight layers SLI.

- Construction of an aluminium shroud covering the complete test item inside the chamber (cf Fig. 3). This shroud is directly screwed to the cold plate and both are wrapped with a common second (outer) MLI.
- More precise SLI wrapping of the specimens and the resistance heater.
- Extending the resistance heater's wire length (0.3 m => 1.5 m) and minimizing its diameter (AWG 22 => AWG 26).
- Connecting the wires with aluminium (instead of polyimide) tape to the cold plate.
- Installing an MLI shield between the vacuum pump and thermal vacuum chamber vessel.

Especially the shroud connecting to the cold plate and the outer MLI ensure a homogenous temperature boundary condition in the improved setup. It has been tested at cold plate temperatures of -50°C and +50°C showing a maximum temperature deviation between the cold plate and the shroud's top side of -4.2°C and -2.6°C respectively. This reduces to approx. 0°C difference at a cold plate temperature of T_{Sink} = 25°C.

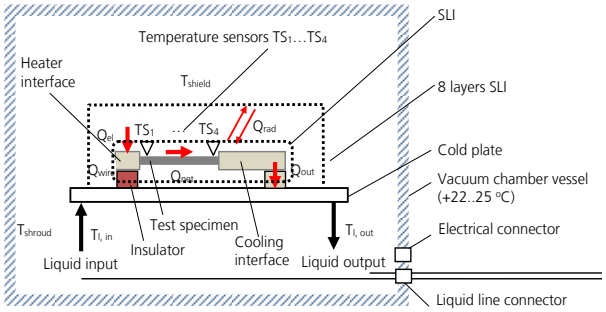

Figure 2: Thermal vacuum test setup as in [3] with three specimen placed adjacently under 8 layers SLI.

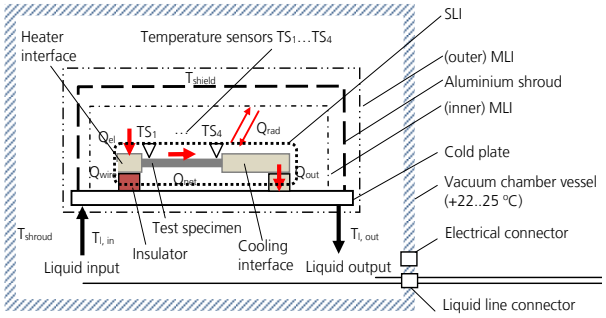

Figure 3: Modified thermal vacuum setup with new shroud and additional MLI layer. Only one specimen tested at a time.

2.2. Validation of the numerical thermal resistance analysis for SLJs

On the basis of the improved thermal vacuum setup the validation of the numerical thermal resistance calculations was repeated for each specimen separately. In a first step the cold plate temperature was set to T_{Sink} = 25°C (298.15 K) and the pressure to $p_{chamber} < 5 \cdot 10^{-6}$ mbar. After reaching thermal equilibrium ($\Delta T < \pm 0.1$ K/h) the resistance heater was set to an output power of 25 mW which is equal to the simulated boundary condition at the flange. As soon as thermal equilibrium was reached again the steady state temperature distribution was determined along the specimen. Subsequently, the same procedure was repeated two more times by increasing the output power at first to 58 mW and then to 110 mW. These levels were selected in order to set for the reference specimen #1 a temperature gradient of approx. 10 K and 20 K between $T_{Heater\text{-}Interface\ (IF)}$ and T_{Sink} respectively. The reason for this is to allow at least a relative comparison between the experiments when the actual heat flux in the specimen is not known. Afterwards the same procedure was repeated two more times for specimen #2 and #3.

A summary of the temperature readings is listed in Tab. 2. Next to the resulting temperature distribution of the present experiment for an applied heater power of Q_{Heater}=58 mW it shows the numerical and experimental results gained in [3] as well as an updated simulation considering the manufactured laminate thicknesses. In the present experiment all temperature readings of sensors TS_1 to TS_4 are offset adjusted on the basis of steady-state readings (initial conditions: heater turned off and cold plate controlled at 25°C).

At first, in order to evaluate the minimisation of the parasitic heat fluxes, the total thermal resistance of each specimen is calculated as following:

$$R_t = \frac{\Delta x}{\lambda \cdot A} = \frac{\Delta T}{\dot{Q}} \qquad (1)$$

Herein ΔT is the temperature gradient between the heater-sided and the sink-sided flange ($TS_{Heater\text{-}IF}$ and TS_{Sink}), Δx is the distance between the flanges, λ is the specimen's effective thermal conductivity and A the specimen's cross section. In [3], with the heater power set to 100 mW for specimen #1 and a temperature increase of 13.26 K, the thermal resistance of the entire specimen calculated to $R_{t,Heater\text{-}Sink\ \#1[3]}$ = 13.26/0.1 = 132.6 K/W. For the present improved experimental setup the total thermal resistance is $R_{t,Heater\text{-}Sink\ \#1}$ = 10.06/0.058 = 173.4 K/W, which is treated as equivalent to 24% reduction of parasitic heat fluxes compared to $R_{t,Heater\text{-}Sink\ \#1[3]}$. Also for specimens #2 and #3 the parasitic heat fluxes are reduced by 35% and 22%, respectively.

Because the differently set heater power in the former and present experiment does not allow a direct comparison of the absolute temperature readings, the following discussion focuses on relative comparisons only. For instance the temperature drops $\Delta TS_{1\text{-}2}$ and $\Delta TS_{3\text{-}4}$ on specimens #1 and #3 should pairwise differ by a factor of 1.5. Comparing those of the present experiment the factor in question is 1.25 for both. This is in the same range as found in the former experiment [3]. Comparing the simulated and experimental results of the present investigation and in [3] for $\Delta TS_{2\text{-}3}$, they show very similar pairings for specimen #2 and #3. For specimen #1 the present experimental results agree less with the simulation. Though, in general the results seem to have improved over the investigations in [3].

Table 2: Simulated temperature distribution along the single-lap joint specimen (cf Fig. 1) and experimental results of [3] compared to the experimental results of present (improved) setup (Q_{Heater}=58 mW) and simulation which considers the laminate thicknesses as manufactured. All temperature readings are in Kelvin and with an accuracy of ±0.1 K.

Spec. No.	Result	Q_{Heater}	$TS_{Heater-IF}$	TS_1	TS_2	TS_3	TS_4	TS_{Sink}	ΔTS_{2-3}	ΔTS_{1-2}	ΔTS_{3-4}	$\frac{\Delta TS_{1-2}}{\Delta TS_{3-4}}$
#1	Sim. [3]	25 mW	308.33	307.67	302.69	301.32	298.63	298.15	1.37	4.98	2.69	1.85
	Exp. [3]	100 mW	311.57	309.69	304.40	303.08	299.10	298.31	1.32	5.29	3.98	1.33
	Present Sim.	25 mW	307.74	307.00	302.40	301.15	298.61	298.16	1.25	4.60	2.54	1.81
	Present Exp.	58 mW	308.28	306.87	302.58	301.64	298.78	298.22	0.94	4.29	2.86	1.50
#2	Sim. [3]	25 mW	307.76	307.10	302.79	300.95	298.63	298.15	1.84	4.31	2.32	1.86
	Exp. [3]	100 mW	310.23	307.91	304.08	302.26	299.09	298.35	1.82	3.83	3.17	1.21
	Present Sim.	25 mW	306.35	305.70	302.08	300.38	298.59	298.16	1.70	3.62	1.79	2.02
	Present Exp.	58 mW	308.76	306.97	303.18	301.54	298.90	298.14	1.64	4.38	2.64	1.74
#3	Sim. [3]	25 mW	304.96	304.52	301.20	300.29	298.50	298.15	0.91	3.32	1.79	1.86
	Exp. [3]	100 mW	308.64	307.21	303.04	302.07	298.83	298.43	0.97	4.17	3.24	1.29
	Present Sim.	25 mW	304.44	303.95	300.91	300.11	298.45	298.16	0.80	3.04	1.66	1.83
	Present Exp.	58 mW	305.92	305.37	302.63	301.12	298.83	298.28	0.76	3.44	2.29	1.50

Table 3: Est. errors due to deviations between the manufactured and simulated SLJ specimen as well as the simulated temperature deviation at $TS_{Heater-IF}$.

Parameter		Spec. No.	Absolute error	Relative error	Sim. temp. deviation at $TS_{Heater-IF}$
Sensor distance dx		#1, #3	37 mm ±0.5 mm	1.4%	≈0.14 K
		#2	32 mm ±0.5 mm	1.5%	≈0.14 K
Laminate width W		#1, #2	20 mm ±0. 1 mm	0.5%	≈0.06 K
		#3	30 mm ±0.1 mm	0.3%	≈0.02 K
Thickness of struct. adhesive		all	0.1 mm ±0.05 mm	50%	≈0.15 K
Laminate thickness	t_{lam1}		0.25 mm ±0.05 mm	20%	≈1.6 K
	t_{lam2}		0.50 mm ±0.05 mm	10%	≈0.4 K
	t_{lam1+2}				≈2.0 K
Temperature T_{Sensor}			25°C ± 0.1°C	0.4%	n.a.

2.3. Results of the validation experiments and recommendations for further design improvements

The present experimental setup showed a significant reduction of parasitic heat fluxes compared to [3]. This is attributed to the additional shroud and MLI layer in the experimental setup which ensures a homogenous temperature environment at 25°C. On the other hand the heat flux in the specimen is unknown which does not allow comparing the absolute temperature readings. Further these are not consistent to each other, and so they are still considered as not useful for any validation or a reliable calculation of the temperature distribution in the SLJ specimen and their thermal resistance.

For improvements Tab. 3 lists an estimation of the deviations between the manufactured and simulated SLJ specimen. To these deviations corresponds an error in the numerically calculated temperature deviation at $TS_{Heater-IF}$. The relative errors are mostly small, but because of the very thin laminates and adhesive layer in the SLJ a deviation between the assigned and manufactured thickness can result in a significant relative error. However, only the laminates' thickness has a significant influence on the temperature distribution and the derived thermal resistance. Considering this in the updated simulation resulted in a temperature decrease of up to 1.41 K at $TS_{Heater-IF}$ for specimen #2.

Summarising, the following improvements are suggested for the experimental design:

1. Implementation of two calorimeters (one heater-sided and one sink-sided) in order to measure the actual heat flux in the specimens (remember: $\lambda_{Laminate}$ was only calculated from the manufacture's data sheet).
2. The laminate thickness should be significantly enlarged, id est by a factor of 10. This will minimise the specimen's thermal resistance as well as the relative error due to thickness deviations (cf Tab. 3).

3. AN ALTERNATIVE SEMI-ANALYTICAL MODEL FOR THE COMBINED STRUCTURAL-THERMAL ANALYSIS

Lange introduced in [3] a simple analytic formula (based on a resistance network) for the calculation of the temperature drop over a SLJ and its derived effective thermal resistance, respectively. As this formula did not proof to be generally applicable, in the following a semi-analytic method is presented that actually combines the structural and thermal analysis of a SLJ. Further it will lead to a finite element model formulation which is not anymore based on a combined 2D/3D FE simulation technique but on a 1D „thermal resistance element".

The new method should allow the structural engineer to derive for a certain structural design the corresponding effective thermal resistance with minimal additional effort and predict its actual value with a precision of ±7.5% (TBC). It should not influence the structural calculations negatively.

In order to determine analytically a SLJ's thermal resistance the new method will require two steps:

1. Analytical calculation of the SLJ's OOP heat flux distribution in the adhesive layer analogue to the maximum shear-stress calculation (paragraph 3.1).
2. Deriving from the maximum OOP heat flux (step 1) the thermal resistance of the SLJ from (paragraph 3.2).

3.1. A shear-stress-analogue analytical calculation of the out-of-plane heat flux distribution in SLJs

Fig. 4 a) depicts the SLJ as before with a constant heat flux Q applied, a jointed length L_j and width W = 20 mm, and an adhesive layer of thickness t_a. Important to note is that hereinafter both adherents have the same thickness $t_{lam1} = t_{lam2} = t_{lam}$. This is the same configuration which was simulated in [3]. On the basis of that FE model the present investigation applies the same one but with a refined jointed zone, id est the elements between x = $-L_j/2$ and x = $+L_j/2$ have only one third of the length and width as before.

The SLJ's OOP heat flux (zFlux) distribution simulated with the refined model, Fig. 4 b), shows that increasing the jointed length from L_j = 10 mm to L_j = 20 mm leads to a reduction of zFlux to basically Zero in the middle of the joint while the maximum heat flux at the edges of the adhesive layer barely differs. Because both adherents have the same thickness of $t_{lam1} = t_{lam2}$ = 0.2 mm (2 mm), but a slightly differing thermal conductivity, the resulting curves are slightly asymmetric with $\tau_{a,max}(-L_j/2) < \tau_{a,max}(+L_j/2)$. Further, Fig. 4 b) illustrates that an increased laminate stiffness ($E_{lam} \cdot t_{lam}$) leads to reduction of the heat flux peaks while the mean z-directional heat flux $\overline{zFlux} = \bar{q}_z = const.$

The curves in Fig. 4 c) depict the shear stress distribution in the adhesive layer of an SLJ for different jointed length and are described by a homogenous differential equation of second order with the following solution [7]:

$$\tau_a = \bar{\tau}_a \cdot \frac{\rho}{2} \cdot \left[\frac{\cosh\left(\frac{\rho x}{L_j}\right)}{\sinh\left(\frac{\rho}{2}\right)} - \frac{(1-\psi)\cdot \sinh\left(\frac{\rho x}{L_j}\right)}{(1-\psi)\cdot \cosh\left(\frac{\rho}{2}\right)} \right] \qquad (2)$$

Herein $\bar{\tau}_a$ is the constant average shear stress in the jointed area, ρ is a characteristic number of the glued joint and ψ is the adherents' stiffness ratio:

$$\bar{\tau}_a = \frac{F_x}{L_j \cdot W} \qquad (3)$$

$$\rho^2 = (1+\psi)\cdot G_a \cdot L_j^2 / (E_{lam1} \cdot t_{lam1} \cdot t_a) \qquad (4)$$

$$\psi = \frac{E_{lam1}}{E_{lam2}} \cdot \frac{t_{lam1}}{t_{lam2}} \qquad (5)$$

Both, Fig. 4 b) and Fig. 4 c) show qualitatively very similar curves and the same behaviour when the laminate thickness is increased or the jointed length is extended. Also the asymmetry due to a different stiffness ratio and/or thermal conductivity ratio, respectively, is found in both graphs.

These similarities suggest that a substitution of the

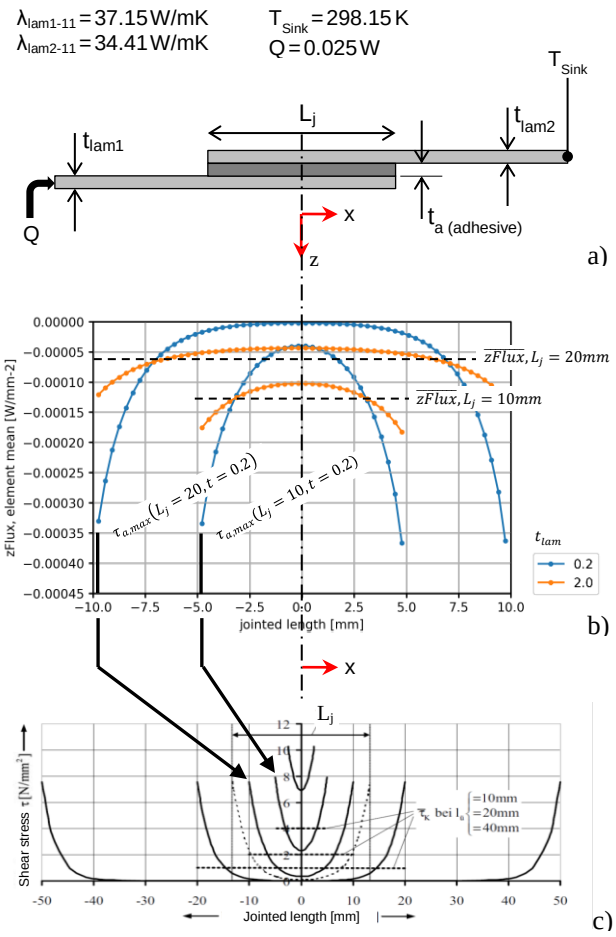

Figure 4: a) SLJ configuration for the analytical and numerical analysis; b) Simulated element mean OOP (z) heat flux distribution in the adhesive layer of a SLJ for a jointed length of L_j =10 mm and L_j =20 mm; c) Shear stress distribution in the adhesive layer of a SLJ for different jointed length L_j (after [7]).

mechanical parameters in Eqs. 2-5 with thermal ones will lead to an analytical description of the OOP heat flux distribution in the adhesive layer [3] that agrees with the numerical simulation in Fig. 4b). Accordingly the following parameters (Tab. 4) are substituted:

Table 4: Substitution of mechanical parameters for the analytical calculation of the OOP heat flux distribution.

Mechanical parameter:	Thermal parameter:
τ_a	$\dot{q}_z$
$\bar{\tau}_a$	$\bar{\dot{q}}_z$
F_x	Q
G_a	$\frac{\lambda_{adhesive}}{0.5\cdot(\lambda_{lam_{13}}+\lambda_{lam_{23}})}$
E_{lam1}	$\lambda_{lam_{11}}/\lambda_{lam_{13}}$
E_{lam2}	$\lambda_{lam_{21}}/\lambda_{lam_{23}}$

In order to compensate for modelling assumptions contained in Eq. 2 the thickness of the adhesive layer t_a is adapted according to the laminates' thickness and the characteristic number of the glued joint (Eq. 4). The results is an effective thickness $t_a = t_{effect.}$ (Eq. 4).

Considering this Fig. 5 shows the evaluated semi-analytic OOP heat flux distribution in the adhesive layer (Eq. 2, mechanical parameters substituted) together with the corresponding numerical results as already presented in Fig. 4 b). Due to the numerical discretisation the zFlux is evaluated in the centre of the finite elements as an element mean value and leading to a small offset at the edges of the jointed zone ($x = -L_j/2$ and $x = +L_j/2$).

The agreement of the semi-analytically with the numerically calculated OOP heat flux distribution in the adhesive layer is for both presented cases very good (maximum deviation <7.5%). Similarly the results for several additional cases, which are not presented for brevity, show a very good agreement. These cases are: various laminate thickness (0.1 mm – 5.0 mm), L_j = 15 mm, W = 30 mm and $\lambda_{lam21} = 2 \cdot \lambda_{lam11}$.

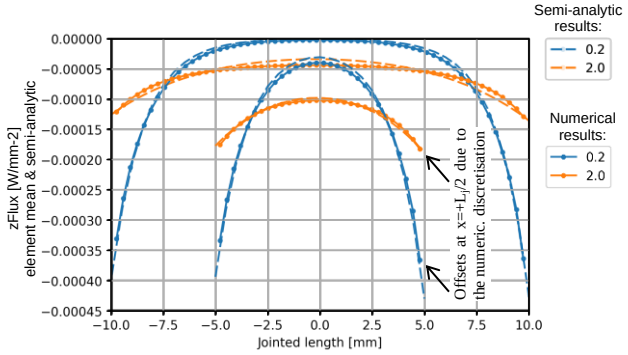

Figure 5: Comparison of the OOP heat flux distribution in the adhesive layer of a 10 mm and 20 mm SLJ. Dashed lines represent the semi-analytical solution (Eq. 2 w/ thermal parameters), full lines the numerical solution.

As an exception, the increase of the adhesive's conductivity by a factor of five leads to deviations lager than +/- 7.5%.

3.2. Derivation of a SLJ's thermal resistance from its characteristic out-of-plane heat flux peaks

Paragraph 3.1 suggested how the characteristic OOP heat flux distribution in the adhesive layer of an SLJ can be expressed for a broad number of cases by a semi-analytical formula which is analogue to the shear-stress calculation. This does not allow the calculation of an SLJ's thermal resistance and the connected temperature drop yet. For that Fig. 6 shows as a function of the adherents' laminate thickness t_{lam} a comparison of both, the maximum OOP heat flux through the adhesive layer (evaluated at $x = -L_j/2$) multiplied by a factor of 10^4 and the temperature drop between $x = -L_j/2$ and $x = +L_j/2$. Although the curves' units do not comply, they show a similar trend. The same kind of correlation is also found when parameters as studied in paragraph 3.1 are changed. Again a significant increase of the adhesive's thermal conductivity results in a less good agreement. Eventually, by subtracting a constant from the 'zFLux_max_numeric–equivalent deltaT' curve, the sought temperature drop over the SLJ and its thermal resistance will be obtained.

Concluding, the presented approach allows to derive for a given thermal load (Q) analytically (shear-stress-analogue) an SLJ's thermal resistance and the connected temperature drop from the maximum OOP heat flux in the adhesive layer as a function of all defining geometrical (t_{lam}, $t_{adhesive}$, L_j, W) and material parameters (E_{lam}, λ_{lam}, $\lambda_{adhesive}$).

In future it is planned to revise the current definition of the effective laminate thickness $t_{effect.}$ (=> curve fitting) and the influence of an increased adhesives' thermal conductivity. Also the mapping approach as introduced in Fig. 6 needs to be further studied and validated before possibly being implemented in a combined structural-thermal model for concurrent engineering purposes.

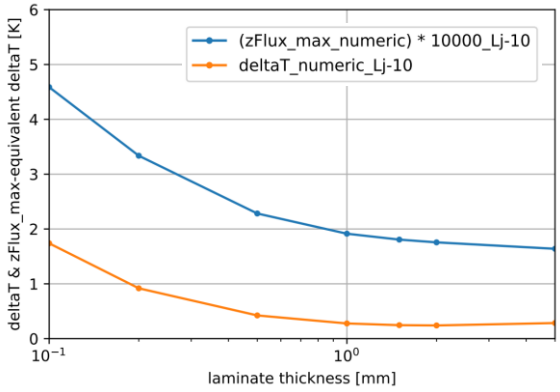

Figure 6: Correlation of the maximum OOP heat flux in the adhesive layer (at $x = -L_j/2$) with the temperature drop over an SLJ (L_j = 10 mm and 0.1 mm < t_{lam} < 5mm).

4. Acknowledgements

The author wants to express to Eugen Mikulz and Kaname Sasaki (both DLR Bremen) his sincere appreciation for the very helpful test support.

5. References

[1] A. Pickering, ESA Concurrent Design Facility, [January 23, 2018], http://esamultimedia.esa.int/docs/cdf/CDF_infopack_2017.pdf.

[2] M.R. Kulkarni, R.P. Brady, A model of global thermal conductivity in laminated carbon/carbon composites, Composites Science and Technology 57 (1997) 277–285.

[3] M. Lange, V. Baturkin, C. Hühne, O. Mierheim, Simulation and measurement of thermal fluxes in load-bearing bonded FRP single-lap joints, in: Proc. of 14th European Conference on Spacecraft Structures, Materials & Environmental Testing, Toulouse, France, 2016.

[4] L.N. McCartney, A. Kelly, Effective thermal and elastic properties of [+θ/−θ]s laminates, Composites Science and Technology 67 (2007) 646–661.

[5] M.N. Parolis, W. Pinter-Krainer, Current and future techniques for spacecraft thermal control, ESA Bulletin (1996) 73–83.

[6] V. Baturkin, Effect of wires junction temperature variation for MTS temperature sensors PT100, For internal use only, 2016.

[7] H. Schürmann, Konstruieren mit Faser-Kunststoff-Verbunden, Springer, Berlin Heidelberg, 2005.